



## ANALYTICAL SIMULATIONS ON STRUCTURAL EXPERIMENTS OF ONE-STORY ONE-BAY R/C MOMENT-RESISTING FRAMES WITH NON-STRUCTURAL WALLS

R.H. Yoon<sup>(1)</sup>, Y. Sanada<sup>(2)</sup>, T. Akahori<sup>(3)</sup>

<sup>(1)</sup> JSPS Research Fellow, Osaka University, Japan, Yoon\_rokhyun@arch.eng.osaka-u.ac.jp

<sup>(2)</sup> Associate Professor, Osaka University, Japan, sanada@arch.eng.osaka-u.ac.jp

<sup>(3)</sup> Former Graduate Student, Osaka University, Japan, takumiakahori@gmail.com

### Abstract

Reinforced concrete (R/C) buildings are often constructed monolithically with non-structural walls. Several past studies verified that monolithic non-structural walls significantly affected the structural performance of R/C moment resisting frames. Severe damage to non-structural walls was observed in a lot of R/C buildings not only after the 2011 off the Pacific coast of Tohoku, Japan earthquake but also earthquakes in other countries. This study mainly focuses on R/C non-structural walls used for exterior/partition walls in typical residential buildings in Japan. Cyclic loading tests were carried out using three 1/2.5 scale, one-story, one-bay R/C moment resisting frame specimens with/without non-structural walls which were monolithically constructed or structurally isolated by seismic slits. As a result, the isolated wall as well as the monolithic wall significantly increased the strength of the moment resisting frame specimen. Furthermore, this study presents analytical models to simulate the experimental results and to clarify the effects of the non-structural walls on the overall performance of the test specimens. The test specimens were replaced by line elements with the multi-spring models. In particular, however, the specimen with the isolated wall with the seismic slits was modeled considering tie bars provided between the main frame and the non-structural wall. The analytical simulations generally showed good agreements with the experimental results. In conclusion, the analytical models proposed in this study are effective to simulate the seismic performance/behavior of R/C moment-resisting frames with the typical non-structural walls used in Japan.

*Keywords: Non-structural Wall, Structural Analysis, Multi-spring Model*

### 1. Introduction

Reinforced concrete (R/C) buildings are normally designed considering structural components, while they are often constructed monolithically with non-structural components. Severe damage to non-structural walls was observed in a lot of R/C buildings not only after the 2011 Great East Japan Earthquake but also earthquakes in other countries, as shown in Figure 1 [1, 2]. Moreover, several past studies have reported that such non-structural walls affected the seismic performance of R/C structure [3, 4]. However, no design methodology has been completed to consider structural effects of non-structural walls.

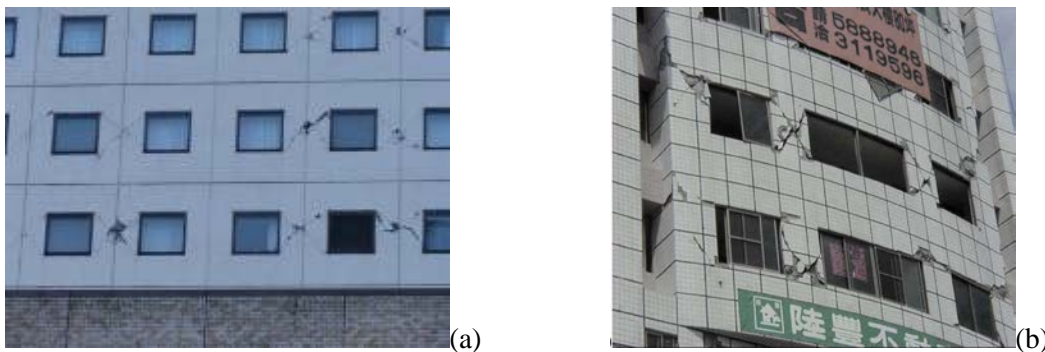


Fig. 1 – Damage to non-structural walls observed:  
(a) The 2011 Great East Japan Earthquake (b) The “921” Taiwan Earthquake

The authors carried out a series of laboratory tests to obtain fundamental data on the seismic behavior of non-structural walls [5]. The tests were planned using three 1/2.5 scale, one-story, one-bay R/C moment resisting frame specimens with/without non-structural walls, which were monolithically constructed or structurally isolated by seismic slits. The experimental results showed that the strength and initial stiffness were influenced by the non-structural walls and tie-bars which were arranged at the wall-frame boundaries. In particular, it was experimentally found that the strengths of the specimens with the monolithic and isolated non-structural wall should be evaluated considering oblique cross-sections critical to flexural yielding and existence of tie-bars, respectively.

Therefore, the purpose of this paper is to propose analytical models to simulate the experimentally observed behavior/performance of the specimens with the non-structural walls. The verification of the proposed models were also performed through comparisons between the experimental results and the numerical simulations.

## 2. Experimental Investigation

### 2.1 Outline of experimental specimens

Figure 2 shows the typical floor framing plan and elevations of a prototype building in this study. Three 1/2.5 scale, one-story, one-bay R/C moment resisting frame specimens (named BF for one of the specimens without non-structural walls) were designed to represent the 2nd-story partial frame in the prototype building, as summarized on Table 1. Figure 3 shows the dimensions and reinforcement details of the specimens. The dimensions of column and beam were 300 mm x 320 mm and 180 mm x 280 mm, respectively. The story height and span length were 1,200 mm and 2,250 mm. Table 2 summarizes the combination of test parameters. Two of the specimens had non-structural walls which were monolithically constructed and structurally isolated by seismic slits (named WF and WFs, respectively). In the case of WFs, a small amount of tie bars (D4@160) were provided for the seismic slits to prevent out-of-plane deformation of the wall according to the Japanese guideline [6]. The tested cylindrical compressive strength of the concrete and the properties of the reinforcement are shown in Tables 3 and 4.

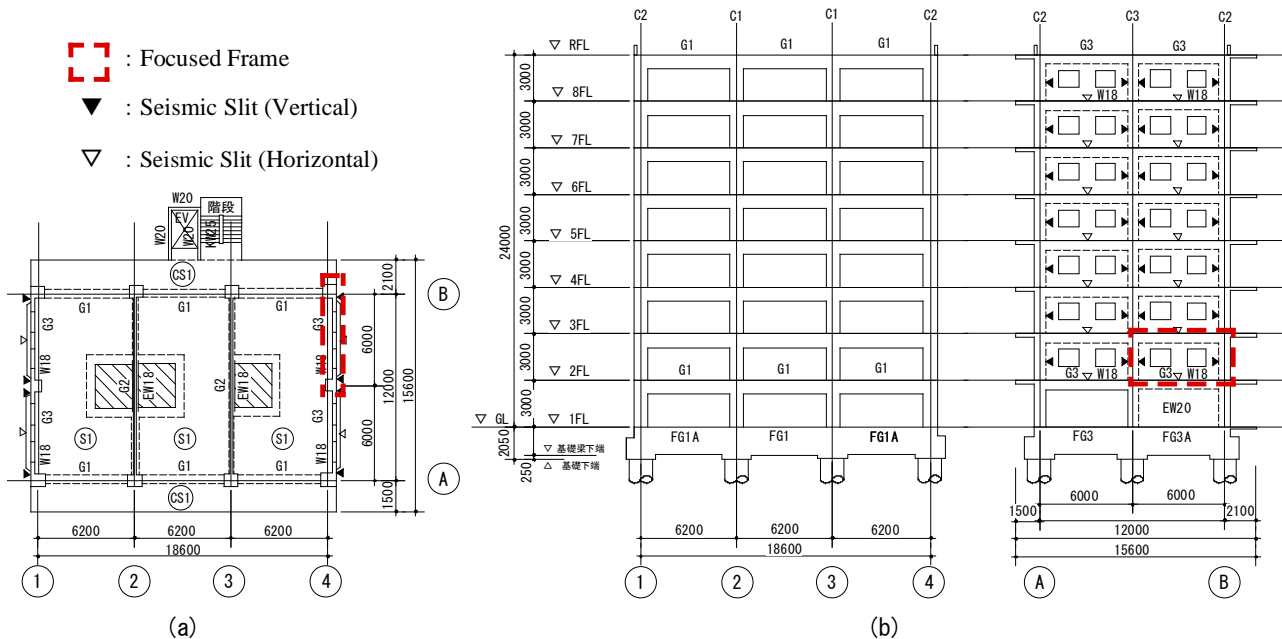


Fig. 2 – Typical floor framing plan and elevations of prototype building :

(a) Typical floor framing plan, (b) Framing elevations along the axes of (A) · (B)/(1) · (4)

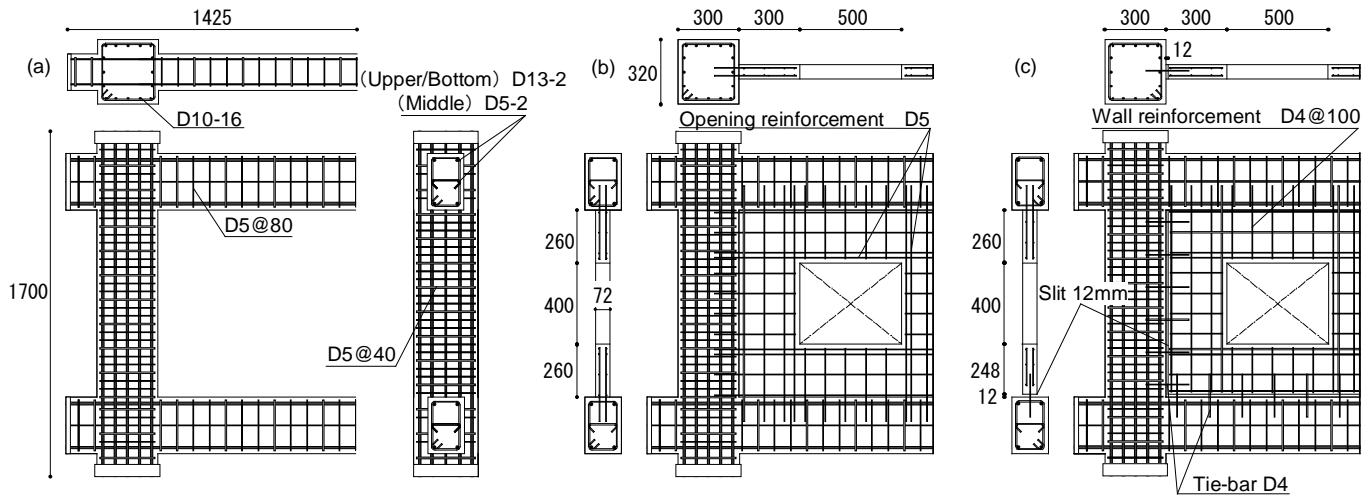


Fig. 3 – Dimensions and reinforcement details of the specimens: (a) BF, (b) WF, (c) WFs

Table 1 – Specifications of members

		Prototype	Specimen
Beam	B×D	450×700	180×280
	Longitudinal rebar	6-D25 ( $p_{tb} = 0.48$ )	4-D13 ( $p_{tb} = 0.50$ )
	Shear reinforcement	2-D13@200 ( $p_{wb} = 0.28$ )	2-D5@80 ( $p_{wb} = 0.31$ )
Column	B×D	750×800	300×320
	Longitudinal rebar	14-D25 ( $p_{tc} = 0.34$ )	16-D10 ( $p_{tc} = 0.34$ )
	Shear reinforcement	D13@100 ( $p_{wc} = 0.28$ )	D10@40 ( $p_{wc} = 0.31$ )
Wall	Thickness	180	72
	Vertical and Horizontal reinforcement	D10@200double	D4@100double
	Reinforcement along perimeter of opening	2-D16	2-D5
	Opening ratio*	–	0.4

$p_{tb}$  : Tensile reinforcement ratio of beam,  $p_{tc}$  : Tensile reinforcement ratio of column

$p_{wb}$  : Shear reinforcement ratio of beam,  $p_{wc}$  : Shear reinforcement ratio of column

\* Opening ratio is defined by  $r_o = (h_o l_o / h l)^{1/2}$

( $r_o$  : opening ratio,  $h_o / l_o$  : height/length of opening,  $h / l$  : story height/span length) [7]

Table 2 – Experimental parameters

Specimen	Non-structural Wall	Slit
BF	Without	Without
WF	With	Without
WFs	With	With

Table 3 – Material properties of concrete

Specimen	Compressive strength (N/mm <sup>2</sup> )	Elastic modulus (kN/mm <sup>2</sup> )
BF	33.5	25.7
WF	35.5	26.5
WFs	33.4	26.5

Table 4 – Material properties of reinforcement

	Yield stress(N/mm <sup>2</sup> )	Tensile strength(N/mm <sup>2</sup> )	Elastic modulus (kN/mm <sup>2</sup> )
D4	320	499	168
D10	313	501	163
D10	381	519	179
D13	391	554	185

## 2.2 Experimental Methods

The specimens were tested using the loading system in Osaka University. A test set-up in the loading system is shown in Fig. 4. The specimens were mounted onto pin supports in the loading system which consisted of one horizontal hydraulic jack and two vertical ones, as shown in Fig. 4. Every specimen was subjected to cyclic lateral loading under a constant axial load of 576 kN ( $N/N_0 = 0.1$ , N: axial load,  $N_0$ : compressive strength of the columns). Incremental loads were controlled by a drift ratio, R (rad.), ratio of inter-story drift to the center-to-center distance between the upper and lower beams. The applied loading history in the lateral direction is illustrated in Fig. 5.

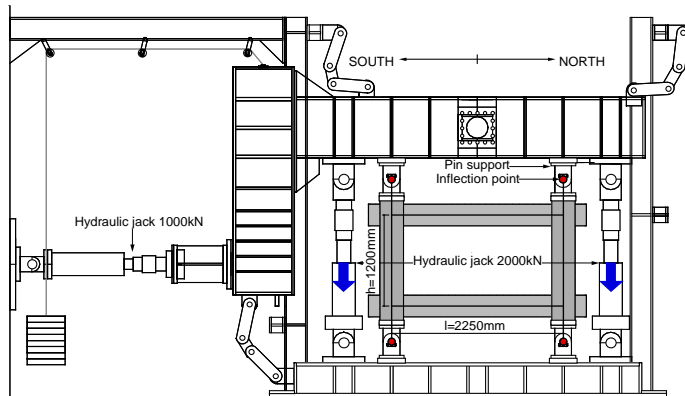


Fig. 4 – Test set-up and loading system

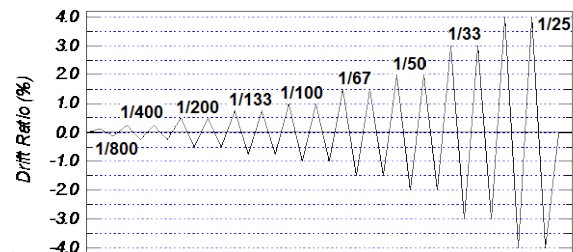


Fig. 5 – Lateral loading history

## 2.3 Experimental Behavior

Figures 6 and 7 compare the lateral force vs. drift ratio relationships and crack patterns among three specimens. Symbols on the lateral force vs. drift ratio relationships mean drifts at the mechanism formation ( $\blacktriangle$ ), maximum strength ( $\bullet$ ) and ultimate state with buckling of beam longitudinal reinforcement ( $\times$ ), respectively. Behavior of each specimen throughout loading is summarized in the following.

### 2.3.1 Specimen BF (moment resisting frame)

Flexural cracks appeared at the upper and lower beam ends during the first cycle to  $R = 1/800$  rad. The specimen formed a mechanism after flexural yielding at all beam ends in the cycle to  $R = 1/200$  rad., because the stiffness



significantly degraded in the following cycles. Lateral resistance of 71 kN at the mechanism formation was observed at the peak drift in the cycle to  $R = 1/133$  rad. However, the lateral resistance still increased with an increase of lateral drift up to the final loading cycle. This was caused by axial elongation of the beam with the incremental lateral drift, because reactive compression was applied to the beam cross-section due to constraint to the axial elongation by both columns. The maximum strength reached 107 kN at the peak drift of the cycle to  $R = 1/25$  rad., where buckling of longitudinal rebars and spalling of concrete cover were also observed at the beam ends. Lateral resistance of 71 kN estimated under no compression on the beam cross-section according to the Japanese design standards [7] underestimated the experimental resistance, as shown Fig. 6(a).

### 2.3.2 Specimen WF (with non-structural walls monolithically constructed)

Flexural cracks on concrete surface and yielding of horizontal rebars were observed at the spandrel/hanging walls during the first cycle to  $R = 1/800$  rad. Shear cracks and yielding of horizontal rebars were also observed at the flat wall between openings in the same loading cycle. In the following cycle to  $R = 1/400$  rad., the spandrel/hanging walls cracked in shear, then, the flat wall yielded in flexure with spalling of concrete cover. The beam longitudinal rebars began to yield in the cycle to  $R = 1/200$  rad. The specimen seemed to form a mechanism in the following cycle to  $R = 1/133$  rad., because of a significant degradation of the stiffness. Lateral resistance at the mechanism was 268 kN, which was identical to the maximum strength recorded at the peak drift in this cycle. It was about 3.8 times as that of BF.

### 2.3.3 Specimen WFs (with non-structural walls isolated by seismic slits)

Specimen WFs behaved in a similar manner to that of BF until the cycle to  $R = 1/133$  rad. Flexural cracks occurred at the beam ends during the first cycle to  $R = 1/800$  rad. However, damage to the upper beam was locally observed at the beam ends with a length approximately equivalent to the beam depth, which seemed to be affected by existence of the non-structural wall. Lateral resistance of 103 kN was recorded at a mechanism formation during the cycle to  $R = 1/133$  rad., which was about 1.5 times as that of BF. Then, the lateral resistance of specimen rapidly increased after the bottom corner of non-structural wall contacted the column in the cycle to  $R = 1/67$  rad., as shown in Fig. 6(c). As a result, shear cracks occurred on the flat wall between openings. The maximum strength reached 172 kN at the peak drift of the cycle to  $R = 1/33$  rad., where buckling of longitudinal rebars was also observed at the beam ends. Compressive failure of concrete was significant at the beam ends and the corners of openings in the cycle to  $R = 1/25$  rad., which caused a strength drop of the specimen. Focusing on tie bars which were arranged at the wall-frame boundaries, they yielded in tension at the vertical slits during the first cycle of  $R = 1/800$  rad., then fractured at the horizontal slits in the cycle to  $R = 1/100$  rad. The strength and initial stiffness of WFs also increased compared to those of BF.

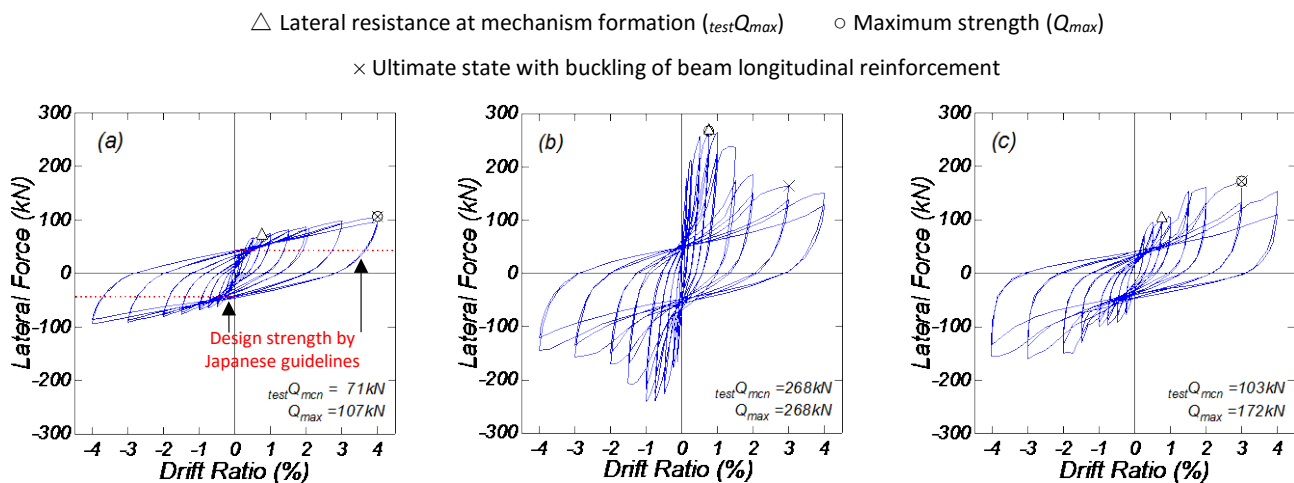


Fig. 6 – Lateral force vs. drift ratio relation: (a) BF, (b) WF, (c) WFs

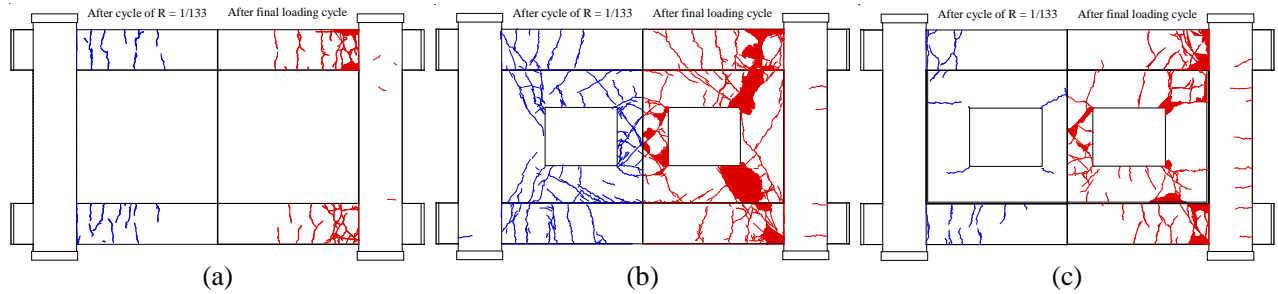


Fig. 7 – Front views of crack patterns: (a) BF, (b) WF, (c) WFs

### 3. Analytical Modeling

#### 3.1 Common modeling of specimens

The experimental results indicated that the structural behavior and seismic performance of the specimens must be evaluated considering interactions between bending moment and axial force for the beams. In addition, appropriate modeling for yield surfaces in the WF and tie-bars in the WFs seemed to be key issues for numerical simulations of the tests, as mentioned above. Thus, the specimens were replaced by idealized numerical models, as shown in Fig. 8, to rationally take into account the above experimental behavior.

The story height and span length in the analytical models were the same as those of the specimens. However, the analytical models represented up to the inflection points of the columns in the upper and lower stories, which located at the center of the pin supports, as shown in Fig. 4. In addition, the pin supports at the ends of columns were assumed to be rigid, as shown in Fig. 8. As for the boundary conditions, a pin supports was attached to each end of the columns in the upper and lower stories. In particular, two pin support in the upper story were configured to have the same displacements in both the x- and y-directions. Applied loads were the same as those in the experiment: cyclic lateral loads were controlled by the inter-story drift ratio  $R$  under constant vertical loads equivalent to 10% of the gross compression capacity of the columns.

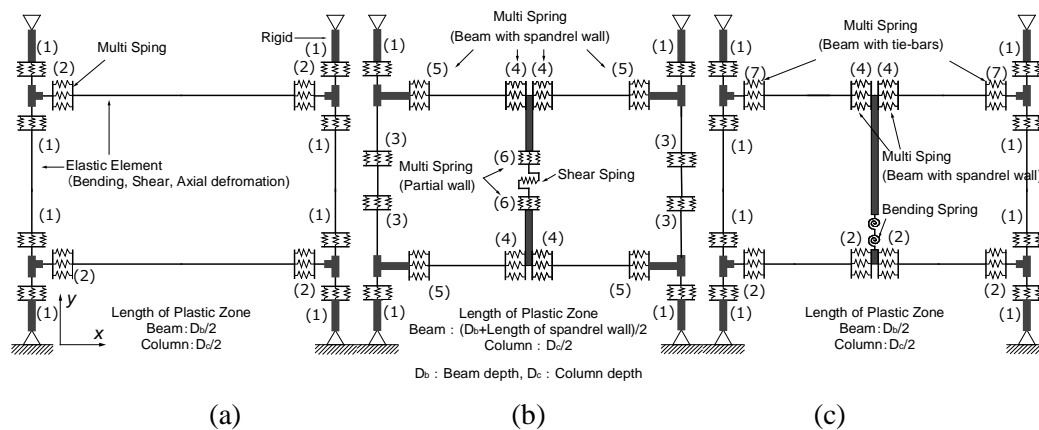


Fig. 8 – Analytical models of the specimens: (a) BF, (b) WF, (c) WFs

A model, called as multi-spring model (MS model) for reinforced concrete columns developed by Lai, Will and Otani was proposed to simulate inelastic behavior of columns [8, 9]. The MS model consists of several uniaxial steel and concrete springs to represent the inelastic flexural rotation and the N-M interaction at the column ends. In this study, the MS model was applied to the analytical models to evaluate the inelastic behavior of the columns and beams in the experiment [5]. Figure 9 shows modeling of the member cross-sections in the MS model, where the numbers corresponded to those in Fig. 8. The cross-sections were replaced by concrete elements with a depth of 20mm and steel elements representing longitudinal rebars.

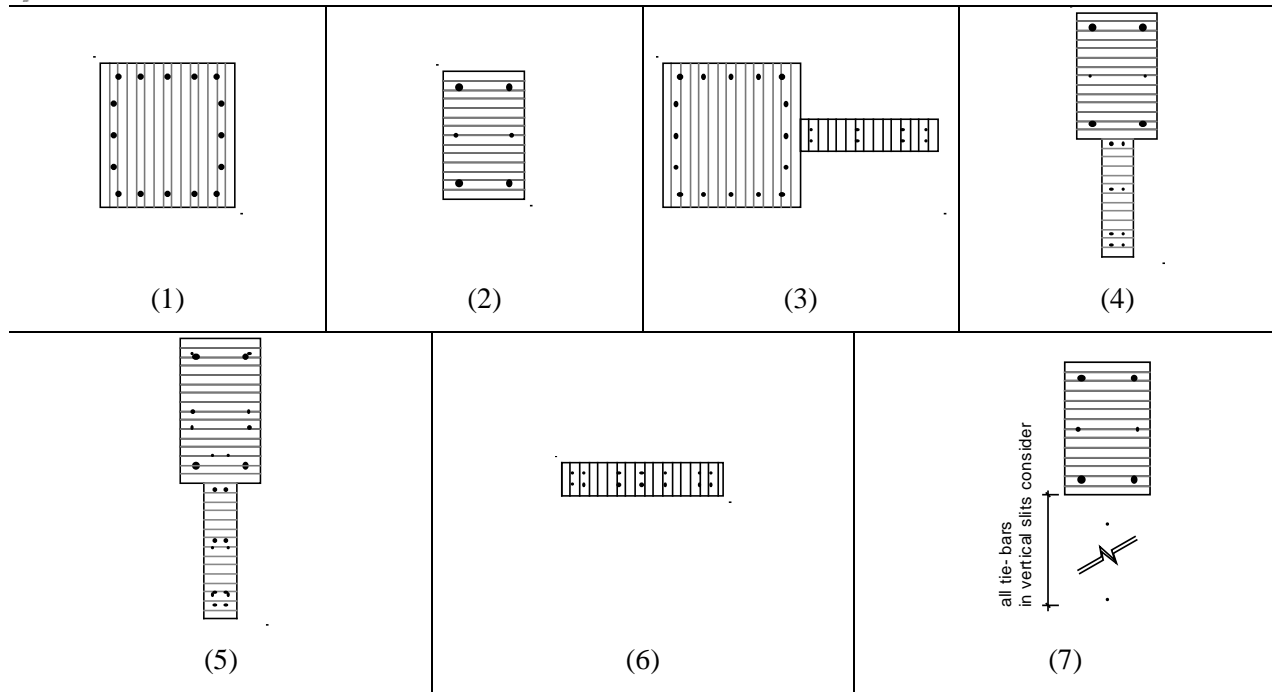


Fig. 9 – Modeling of member cross-sections in the MS model: (1) column, (2) beam, (3) column with wing wall, (4) beam with spandrel/hanging wall, (5) beam with spandrel/hanging wall (oblique cross-section), (6) flat wall, (7) beam with tie-bars

### 3.2 Specific modeling of specimens

#### 3.2.1 Specimen BF (moment resisting frame)

The columns and beams were replaced by a line element which consisted of two MS models at both member ends sandwiching a linear element. Critical sections of the columns and beams in the middle story were defined to be at the beam and column surfaces. Rigid zone at the ends of columns and beams in the middle story were assumed to be within a range from each node to 1/4 of the member depth. Plastic hinge length in the MS model was assumed to be 1/2 of the column and beam depths.

#### 3.2.2 Specimen WF (with non-structural walls)

The columns and beams were modeled by considering the wing and spandrel/hanging walls, respectively. The critical sections of the columns in the mid-story were defined to be at the spandrel/hanging wall ends, as shown in Fig. 10. Furthermore, the critical sections of the beams were assumed an oblique cross-section, as shown Fig. 10, considering the experimental results. The rigid zones at the member ends in the middle story were assumed to be within a range from each node to the critical section. The critical sections and rigid zones in the flat wall between openings were defined to be at the spandrel/hanging wall ends and within a range from each node to the critical section. The plastic hinge length of MS model for the beams was assumed at 1/2 of the whole depth of the beam with spandrel/hanging wall, while that for the columns was modeled in the same manner as that of BF. In addition, the flat wall between the openings was represented by a line element with the MS model and non-linear shear spring. A tri-linear model was applied to the shear spring considering strength deterioration, as shown in Fig. 11. The resistance to shear cracking,  $Q_{cr}$  was evaluated by Equation (1) [10].  $Q_{su}$  was the ultimate shear strength given by Equation (2) [10]. The shear deformation angle at shear cracking,  $R_{cr}$  was theoretically evaluated by Equation (3). The shear deformation angle at the ultimate shear strength,  $R_u$  was assumed to be 0.004rad. based on the Japanese standards [11].

$$Q_{cr} = \left( \frac{0.085 \cdot k_c \cdot (F_c + 500)}{M/(Q \cdot D) + 1.7} \right) \cdot t \cdot j \quad (1)$$



where.  $k_c$ : 0.72,  $F_c$ : concrete strength,  $M/(Q \cdot D)$ : shear span-to-depth ratio,  $t$ : wall thickness,  $j = 7/8 \cdot D$ ,  $D$ : whole length of wall.

$$Q_{su} = \left( \frac{0.053 \cdot p_{te}^{0.23} \cdot (18 + F_c)}{M/(Q \cdot D) + 0.12} + 0.85 \sqrt{p_{wh} \cdot \sigma_{wh} + 0.1 \cdot \sigma_{0e}} \right) \cdot t \cdot j \quad (2)$$

where,  $p_{te} = 100 \cdot a_t / (t \cdot D)$ ,  $a_t$ : sum of the cross-sectional area of the longitudinal reinforcements in the tensile boundary column,  $\sigma_{wh}$ : yield stress of the shear reinforcement,  $p_{wh}$ : shear reinforcement ratio,  $\sigma_{0e}$ : averaged constant axial stress.

$$R_{cr} = Q_{cr} / GA_w \quad (3)$$

where,  $G$ : elastic shear modulus,  $A_w$ : gross cross-sectional area of the flat wall.

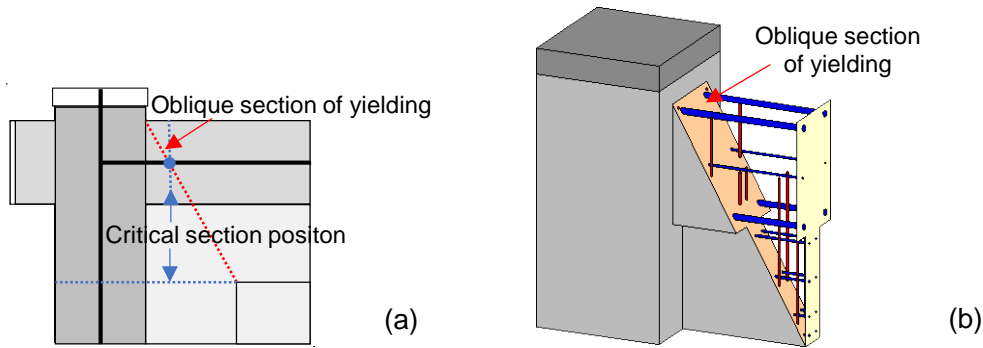


Fig. 10 – Critical section of the specimen WF: (a) 2D image, (b) 3D image

### 3.2.3 Specimen WFs (with non-structural walls isolated by seismic slits)

For the specimen WFs with non-structural walls isolated by seismic slits, the columns and lower beam were modeled in the same manner as those for the specimen BF. The critical sections of the columns and beams in the middle story were defined to be at the beam and column surfaces. The rigid zone at the ends of columns and beams in the middle story were assumed to be within a range from each node to 1/4 of the member depth. The upper beam was modeled considering the presence of tie-bars at vertical slits and the hanging wall that located above the openings. For the MS models in the upper beam ends above the vertical slits, the cross-sections were represented including the tie-bars on the vertical slit, as shown in Fig. 9(7). In addition, the cross-section at the middle of the upper beam considered the hanging wall above the openings, as shown in Fig. 9(4). The plastic hinge length of MS model was assumed to be equal to 1/2 of the column and beam depths, similarly to those of BF. On other hand, relative horizontal displacements between the lower beam and non-structural wall were observed in the experiment; thus, the tie-bars on horizontal slit carried shear forces. The tie-bars of the horizontal slit were replaced by a line element that connected the centers of the upper and lower beams. The flexible height of the line element was assumed to be equal to the clearance of the horizontal slit, considering a rigid zone along the wall panel. Bending springs with the common bilinear model considering the Bauschinger effect, as shown in Fig. 12, were provided at the ends of the line element. The initial stiffness of the bending spring was obtained by multiplying number of tie-bars by the elastic bending stiffness of a tie-bar. The full plastic moment,  $M_u$  was defined as Eq. (4).

$$M_u = \frac{\pi \cdot d^2}{8} \cdot \sigma_y \cdot \frac{4d}{3\pi} \cdot n_s \quad (4)$$

where  $d$ : diameter of tie-bar,  $\sigma_y$ : yield stress of tie-bar,  $n_s$ : number of tie-bar in a horizontal slit.

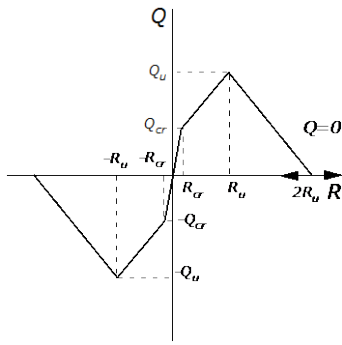


Fig. 11 – Shear spring model considering strength deterioration

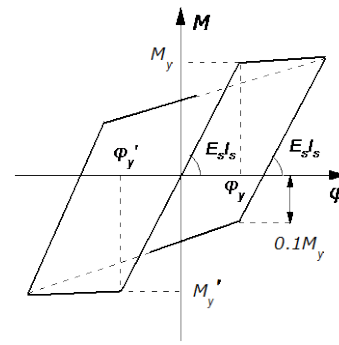


Fig. 12 – Restoring force model for the tie-bars in horizontal slit

### 3.3 Material properties

Figure 13 illustrates restoring force characteristics modeled for concrete and reinforcements for the MS model. The compression behavior of the concrete was evaluated by the Kent and Park model [12], as shown in Fig. 13(a). Meanwhile, the tensile behavior of the concrete was defined to be linear, ranging up to the cracking strength, and to consider tension stiffening. In addition, a bilinear model representing the stress-strain relationship of reinforcements considered the Bauschinger effect. The mechanical properties of concrete and reinforcements were referred to the experimental results, as shown in Tables 2 and 3.

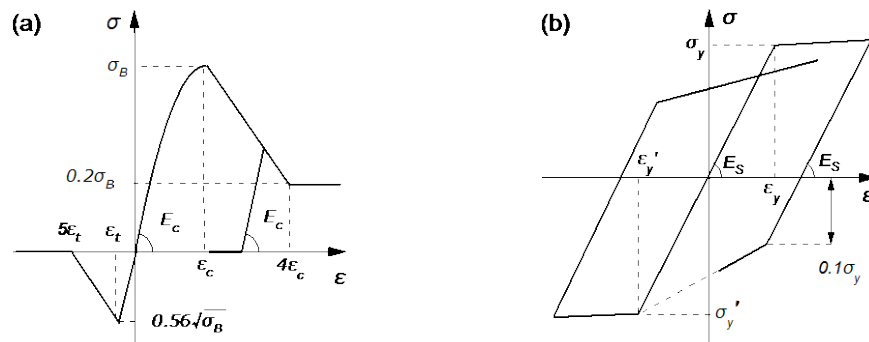


Fig. 13 – Restoring force models: (a) concrete, (b) steel reinforcement

## 4. Simulation Results

### 4.1 Skeleton curve

Figure 14 compares the envelope curves of the lateral force vs. drift ratio relationships from the experiments with the analytical results. Symbols on the lateral force vs. drift ratio relationships mean drifts at initial cracking of beam ( $\blacktriangle$ ), flexural yielding of beam ( $\bullet$ ), and shear failure of flat wall ( $\blacksquare$ ), respectively.

The analytical models for all specimens well evaluated the experimental initial stiffness. In the analytical results, however, the stiffness after flexural cracking that occurred at the beam ends was a little higher in comparison with the experimental results, which resulted in lower drifts at the flexural yielding. Such underestimations attributed to pullout behavior of longitudinal rebars from concrete in the experiments which was not considered in the analyses. Focusing on the analytical results of WF, the flat wall between openings reached the ultimate strength at a small drift ratio, as observed in the experiment. Moreover, compressive failure of concrete was observed at the corners of openings from the cycle to  $R = 1/133$  rad. in the MS model which represented the beams with the spandrel/hanging wall, which was also well agreed with the experimental observations.

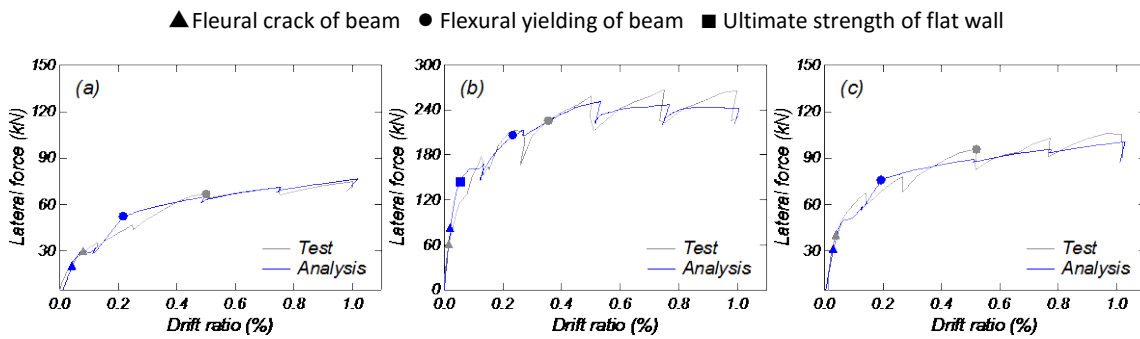


Fig. 14 – Analytical envelope curves and comparisons with the experimental results: (a) BF, (b) WF, (c) WFs

### 4.2 Hysteresis behavior

Figure 15 compares the hysteresis characteristics between the analysis and the experiment for three specimens. The analysis for BF underestimated the experimental hysteretic energy dissipations during small drift angles. However, the shapes of the hysteresis loops in all specimens after yielding were approximately consistent with the experimental results.

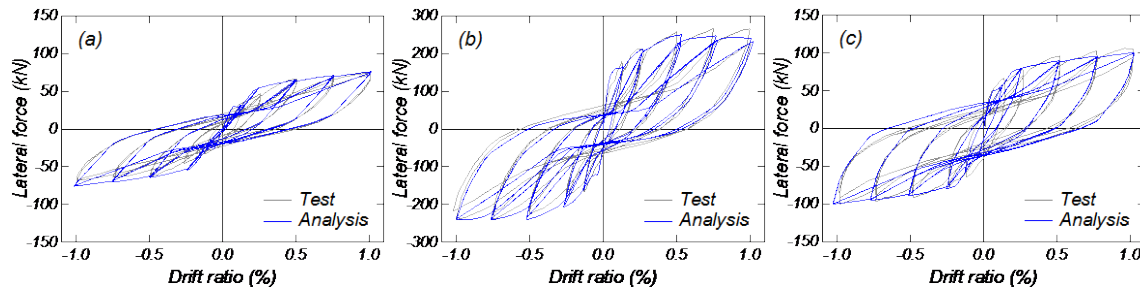


Fig. 15 – Load-displacement relationships and comparisons with the experimental results:

(a) BF, (b) WF, (c) WFs

### 4.3 Axial deformation of beam

Figure 16 compares the axial elongation of upper beam at the peak drifts between the analysis and the experiment for each specimen. The analysis results were approximately consistent with the experimental results. The axial elongation of each specimen increased with an increase of lateral drift. However, the analytical values in the cycle to  $R = 1/100$  rad. underestimated compared to the experimental values. This was caused by the analytical assumptions that the pullout behavior of longitudinal rebars was neglected.

In conclusion, the lateral resistances of the specimens could be evaluated approximately by using MS model that has been placed in the beam members. The analytical models proposed in this study can be judged for assessment of the impact on the axial force of the beam by using MS model, since the skeleton curve obtained in the proposed analytical model was evaluated accurately.

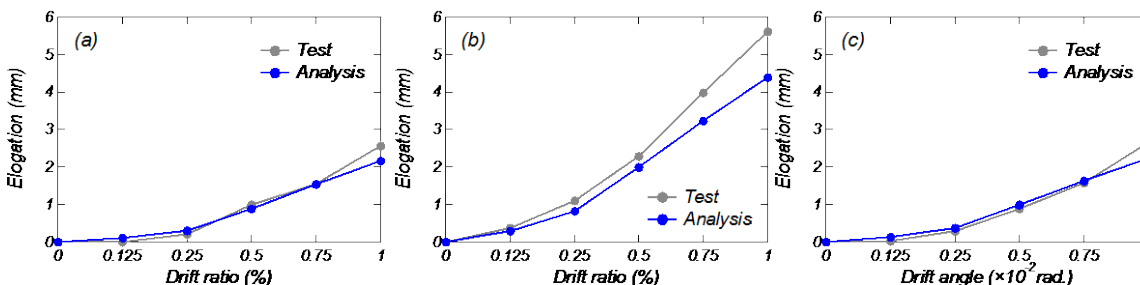


Fig. 16 – Axial elongation vs. drift ratio relationships and comparisons with the experimental results:

(a) BF, (b) WF, (c) WFs



## 5. Conclusions

This paper analytically investigated the effects of R/C non-structural wall with/without seismic slits on the seismic performance of R/C moment resisting frames. The major findings are summarized as follows:

- (1) Adopting the MS model to the beams in the R/C moment resisting frame specimens, the experimental behaviour which was affected by interactions between bending moment and axial force was well simulated.
- (2) Simulating the behavior/performance of the specimen WF which had a monolithic non-structural wall, application of the MS model to oblique critical sections was proposed in this study. Consequently, it was verified that the proposed model could well evaluate the experimental results.
- (3) Simulating the behavior/performance of the specimen WFs which had an isolated non-structural wall with seismic slits, new modeling of tie-bars which were arranged at the wall-frame boundaries were proposed and verified showing good agreements with the experimental results.

## 6. Acknowledgement

This study was supported by Grant-in-Aid for JSPS Fellows Grant Number 15J00625 and special Project for Reducing Vulnerability for Urban Mega Earthquake Disasters, (ii) Maintenance and Recovery of Functionality in Urban Infrastructures, Japan Ministry of Education, Culture, Sports, Science and Technology (MEXT).

## 7. References

- [1] Nishiyama I, Okawa I, Fukuyama H, Okuda Y (2012): Building damage by the 2011 tohoku japan earthquake and coping activities by NILIM and BRI collaborated with the administration. *Proceedings of the International Symposium on Engineering Lessons Learned from the 2011 Great East Japan Earthquake*, 504–515.
- [2] Wallace J, Elwood K, Massone L (2008): Investigation of the axial load capacity for lightly reinforced wall Piers. *Journal of Structural Engineering*, 134(9):1548–1557.
- [3] Orakcal K, Massone L, Wallace J (2009): Shear strength of lightly reinforced wall piers and spandrels. *ACI Structures Journal*, 106(4):455-465.
- [4] Kabeyasawa T, Kabeyasawa T, Kato S, Hosokawa Y (2014): Effect of spandrel and hanging walls on flexural capacity of reinforced concrete columns with wing walls. *10<sup>th</sup> U.S. National Conference on Earthquake Engineering*, Paper ID 115.
- [5] Yoon RH, Sanada Y, Akahori T, Suzuki S, Kuramoto H (2014): Structural experiments of one-story one-bay R/C moment-resisting frames with non-structural walls. *Proceedings of the 16th Japan-Taiwan-Korea Joint Seminar on Earthquake Engineering for Building Structures*, 249-256.
- [6] Architectural Institute of Japan (2010): Recommendation for detailing and placing of concrete reinforcement. *Architectural Institute of Japan*. (in Japanese)
- [7] Architectural Institute of Japan (2010): AIJ standard for structural calculation of reinforced concrete structures. *Architectural Institute of Japan*. (in Japanese)
- [8] Lai S, Will GT, Otani S (1984): Model for inelastic biaxial bending of concrete members. *Journal of Structural Engineering*, 110 (11): 2563-2584.
- [9] Li KN, Aoyama H, Otani S (1988): Reinforced concrete columns under varying axial load and bi-direction lateral load reversal. *Proceedings of the 9<sup>th</sup> world conference on earthquake engineering*, VIII, 537-542.
- [10] Architectural Institute of Japan (1990): Ultimate strength and deformation capacity buildings in seismic design. *Architectural Institute of Japan*. (in Japanese)
- [11] Architectural Institute of Japan (1997): Design Guidelines for earthquake resistant reinforced concrete buildings based on inelastic displacement concept (draft). *Architectural Institute of Japan*. (in Japanese)
- [12] Park R, Priestley MJN, Gill WD (1982): Ductility of square-confined concrete columns. *Journal of the Structural Division*, 108(4): 929-950.